Off-plane x-ray reflection grating fabrication

Thomas J. Peterson, Casey T. DeRoo, Hannah Marlowe, Randall L. McEntaffer, Drew M. Miles, et al.

Thomas J. Peterson, Casey T. DeRoo, Hannah Marlowe, Randall L. McEntaffer, Drew M. Miles, James H. Tutt, Ted B. Schultz, "Off-plane x-ray reflection grating fabrication," Proc. SPIE 9603, Optics for EUV, X-Ray, and Gamma-Ray Astronomy VII, 960317 (21 September 2015); doi: 10.1117/12.2188302

SPIE.

Event: SPIE Optical Engineering + Applications, 2015, San Diego, California, United States

Off-Plane X-Ray Reflection Grating Fabrication

Thomas J. Peterson, Casey T. DeRoo, Hannah Marlowe, Randall L. McEntaffer, Drew M. Miles, James H. Tutt, Ted B. Schultz

University of Iowa, Department of Physics and Astronomy, Van Allen Hall, Iowa City, IA, USA, 52242

ABSTRACT

Off-plane X-ray diffraction gratings with precision groove profiles at the submicron scale will be used in next generation X-ray spectrometers. Such gratings will be used on a current NASA suborbital rocket mission, the Off-plane Grating Rocket Experiment (OGRE), and have application for future grating missions. The fabrication of these gratings does not come without challenges. High performance off-plane gratings must be fabricated with precise radial grating patterns, optically flat surfaces, and specific facet angles. Such gratings can be made using a series of common micro-fabrication techniques. The resulting process is highly customizable, making it useful for a variety of different mission architectures. In this paper, we detail the fabrication method used to produce high performance off-plane gratings and report the results of a preliminary qualification test of a grating fabricated in this manner. The grating was tested in the off-plane 'Littrow' configuration, for which the grating is most efficient for a given diffraction order, and found to achieve 42% relative efficiency in the blaze order with respect to all diffracted light.

Keywords: X-ray spectroscopy, off-plane reflection, X-ray diffraction, grating fabrication

1. INTRODUCTION

The soft X-ray energy range (0.2 - 1.5 keV) contains many transition lines useful for characterizing energetic astrophysical plasmas such as stellar coronae, black hole accretion disks, supernova remnants, and the intergalactic medium.[1] By probing these plasmas with a soft X-ray spectrometer, a highly resolved spectrum with good signal-to-noise can be produced. This spectrum contains information that can be used to determine the temperature, density, ionization state, and metallicity of the plasma. Such a spectra can be obtained using an X-ray grating spectrometer. X-ray grating spectrometers typically consist of three major components: a focusing optic array, a grating array, and a detector array. The focusing optics, usually consisting of nested Wolter-I type optics, collect light from the source and directs it towards a focus several meters down the optical axis. Instead of being allowed to reach the focus, the converging light is intercepted by a grating array. The periodic structure present on the gratings diffracts the converging light based on its wavelength. The diffraction pattern is then imaged with a detector array at the focal plane, and the source spectrum is reconstructed based on the observed diffraction pattern.

X-ray grating spectrometers typically come in three major categories based on the kind of grating employed: transmission, in-plane reflection, and off-plane reflection. A typical X-ray transmission grating is a periodic structure of slatted bars held in place by a support architecture which permits photons to pass through.[2] In-plane X-ray reflection gratings are periodically spaced grooves running perpendicular to the incoming light, resulting in a far-field diffraction pattern in the plane defined by the grating normal and the direction of the incoming light. Off-plane gratings are similar to in-plane gratings, except the grating grooves are oriented quasi-parallel to the incoming light. This results in a conical diffraction pattern at the focal plane, sometimes called the 'arc of diffraction.' Through shaping of the groove facet and controlling the incidence geometry, X-ray gratings can be 'blazed' producing high efficiency in a given order based on diffraction geometry.[3]

The geometry of the off-plane mount offers advantages over its counterparts in an astrophysical context.[4] The largest advantage gained from off-plane gratings over in-plane gratings is that arrays of off-plane gratings do

Address all correspondence to: Thomas Peterson, University of Iowa, Department of Physics and Astronomy, B08 Van Allen Hall, Iowa City, IA, USA, 52242; Tel: +1 319-335-1835; E-mail: thomas-peterson@uiowa.edu

Optics for EUV, X-Ray, and Gamma-Ray Astronomy VII, edited by Stephen L. O'Dell, Giovanni Pareschi,
Proc. of SPIE Vol. 9603, 960317 · © 2015 SPIE · CCC code: 0277-786X/15/$18 · doi: 10.1117/12.2188302

not suffer from vignetting at high order. The resolving power of a grating spectrometer increases when working at higher order, scaling linearly with n, the order number. Stacking gratings at grazing incidence to form an array can result in vignetting for gratings in the in-plane mount, since higher orders are dispersed upwards into the grating above. The off-plane mount disperses high orders out of the plane of incidence where there is no impediment along the optical path.[3]

Off-plane gratings have a 'Littrow' mounting (Figure 1.1) in which the intensity of a particular order or wavelength is maximized. This is realized by using a grating with a blazed triangular groove profile, and mounting the grating such that the projection of the incident light onto the plane orthogonal to the groove direction is along the normal of the triangular facet. In practice, this is done by setting the pitch angle and yaw, or rotation about the grating normal, for a grating to the given facet angle of the grating.[5] The diffraction efficiency is then maximized for diffracted light sharing that projection. At the systems-level, this effect can be used to increase a spectrometer's effective area near particular spectral lines of interest. In terms of the variables in the diffraction equation, the Littrow configuration is realized when $\alpha = \beta = \theta$, where θ is the groove facet angle, α is the reflection angle the top of the arc of diffraction, and the diffraction efficiency peaks for light that would be dispersed at β.

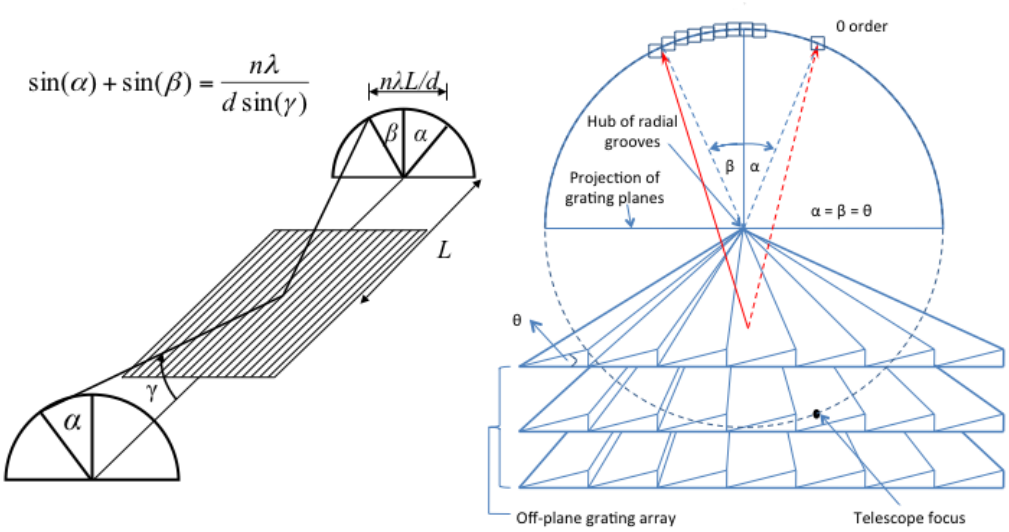

Figure 1.1. An off-plane grating array in the Littrow mounting. Light is preferentially diffracted to β based on the diffraction geometry.[6]

2. FABRICATION REQUIREMENTS

Next generation off-plane grating spectrometers will require customizable gratings for optimized diffraction efficiency and optimal resolution. First, to achieve high spectral resolution the grating grooves must be radially ruled. Without a radial ruled groove pattern, the relative angle between the grooves and the incident X-rays from a converging beam will change over the length of the grating. The variance in this relative angle will result in a variation of azimuthal angle of the diffracted spot, yielding a broad spectral line. With radially ruled gratings, the angle between the X-rays and the grooves is kept constant, dispersing photons of the same wavelength to the same location on the arc of diffraction regardless of the angle of incidence.

The gratings must have specially shaped triangular blazed facets to diffract light preferentially to one side of zero order, maximizing diffraction efficiency. The blaze effect can be used to maximize diffraction efficiency for a given physical section of the arc of diffraction, which corresponds to a range in wavelength space. The groove densities must also be large, in the range from 4,000-10,000 grooves/mm, in order to diffract at X-ray

wavelengths.[7] In order to contribute efficient collecting area for a spectrometer the gratings must be manufactured over areas on the order of 100 cm^2. Finally, the gratings need to exceed the flatness requirements for the optical system. Any deviations from flat will lead to misalignment of the diffracted X-rays, causing broadening of the line spread function at the focal plane.[8] To summarize, a high performance X-ray spectrometer must have gratings with radially fanned grooves, angled 'blazed' facets, high groove densities, large patterned areas, and minimal substrate flatness deviations.

3. FABRICATION PROCEDURE

Off-plane gratings that meet all of these requirements can be manufactured using the ten step microfabrication process shown in Figure 3.1. First, a silicon wafer is sputter coated with a ∼300 Å silicon nitride (SiN_x) hard mask and spin coated with ∼90 Å of NXR-1025 thermal nanoimprint resist. These layers are deposited over a ∼10 Å native silicon dioxide layer present on the substrate (Step 1). Next, a nanoimprint mold with the desired groove density is coated with a mold release agent and cleaned using a three step solvent rinse (Step 2). The mold has the same groove density, radial ruling and size as the final flight grating. However, the mold has a laminar or square wave groove profile and does not have the desired figure quality required for flight gratings. The mold manufacture processing is described in detail in McEntaffer et al. (2013).[6] The mold must be coated with a release agent before imprinting to ease the separation of the mold from the substrate. Imprinting without the release agent can cause damage to the substrate and the transferred pattern on the mold. The pattern is then transferred from the mold to the substrate via thermal nanoimprint lithography(T-NIL). Using a Nanonex-2000 nanoimprinter, the mold is brought in contact with the resist. The substrate is then heated above the glass transition temperature for NXR-1025. A high pressure air cushion presses the mold into the liquid resist. While pressure is still being applied, the substrate is rapidly cooled, transferring the mold's laminar pattern negative into the resist (Step 3). The mold is then separated from the substrate and the substrate is placed in a PlasmaPro NGP80 where two anisotropic reactive ion etches (RIE) are performed to transfer the laminar pattern through the resist and nitride layers (Step 4). To transfer the pattern through the resist, a Ar/O_2 etch is used consisting of 10 sccm of O_2 and 5 sccm of Ar. The nitride etch consists of 50 sccm of CHF_3 held at 100 Watts RF and 10 sccm of O_2 held at 40 Watts RF. The substrate is then submerged in an acetone bath to remove residual resist, leaving strips of silicon nitride matching the mold's groove pattern (Step 5).

Following the acetone bath, the sample is dipped in a buffered hydrofluoric acid (HF) solution which removes the layer of native silicon oxide, exposing the bare silicon wafer (Step 6). The buffered HF solution consists of a 20:1 ratio of a 16% ammonium fluoride (NH_4F) solution and a 49% HF solution. With the silicon oxide layer removed, the sample is ready for an anisotropic wet etch in 20% by weight potassium hydroxide (KOH) solution, which will generate the triangular shaped groove facets (Step 7). In silicon, the KOH etch rate in the <111> crystalline direction is orders of magnitude slower than in other crystallographic directions. This phenomenon can be exploited to preferentially etch along the (111) planes, forming angled grooves with facets along the (111) planes of the etch mask.

The anisotropic etch step allows for fine tuning of the facet angle of the grating grooves based on the crystalline orientation. Commercial silicon wafers are manufactured with a variety of crystalline orientations that define the wafer normal. For instance, the wafer normal of a <100> wafer is the <100> direction of a silicon lattice. Each wafer orientation has a different relative angle between the <111> plane and the wafer normal, allowing the fabrication of gratings with a variety of blaze angles. The grating facet angles for common silicon wafer crystallographic orientations are given in Table 3.1. Silicon foundries are also able to dice silicon ingots off-axis up to 10° from the wafer normal. Using off-axis dicing of wafers with different crystallographic orientations, it is possible to produce any blaze angle within a 1° dicing tolerance.

During the KOH wet etch step, the laminar silicon nitride pattern acts as an etch mask: silicon substrate material is removed between the silicon nitride strips until a (111) plane bounded by a silicon nitride strip is reached, effectively stopping the etch. The silicon nitride mask is then removed using a 49% by weight HF solution which chemically removes silicon nitride without affecting the silicon substrate (Step 8). The resulting grating has the same groove density and radial profile as the original imprint mold but has triangular, blazed facets. However, the produced grating does not meet the optical figure quality requirement, as silicon wafers have global flatness specifications that are outside the requirements needed for co-aligning off-plane gratings. To

Table 3.1. Facet angles achievable using different crystallographic orientations of silicon wafers.

Wafer Orientation	Blaze Angle
<111>	0°
<211>	22.4°
<311>	29.5°
<511>	38.9°
<711>	43.3°
<100>	54.7°

achieve the needed figure, the radially ruled, blazed grating profile is then imprinted into resist on a fused silica substrate via ultraviolet nanoimprint lithography (UV-NIL) (Step 9). In addition to satisfying the figure quality requirements, the UV-NIL step allows for a more efficient manufacturing process because the same silicon grating can be used for multiple imprints. The resist layer must be mechanically durable as it will need to withstand flight conditions. UV-NIL must be used in place of T-NIL as T-NIL will lose the fidelity of the imprinted pattern over time. On the contrary, UV-NIL uses a liquid polymer which cures after exposure to UV radiation, forming long polymer chains which have significantly higher mechanical and thermal stability.[3] A thin X-ray reflective layer such as gold, platinum, or iridium is then deposited over the fused silica sample (Step 10), thus yielding a flight quality, radially grooved, blazed off-plane grating.

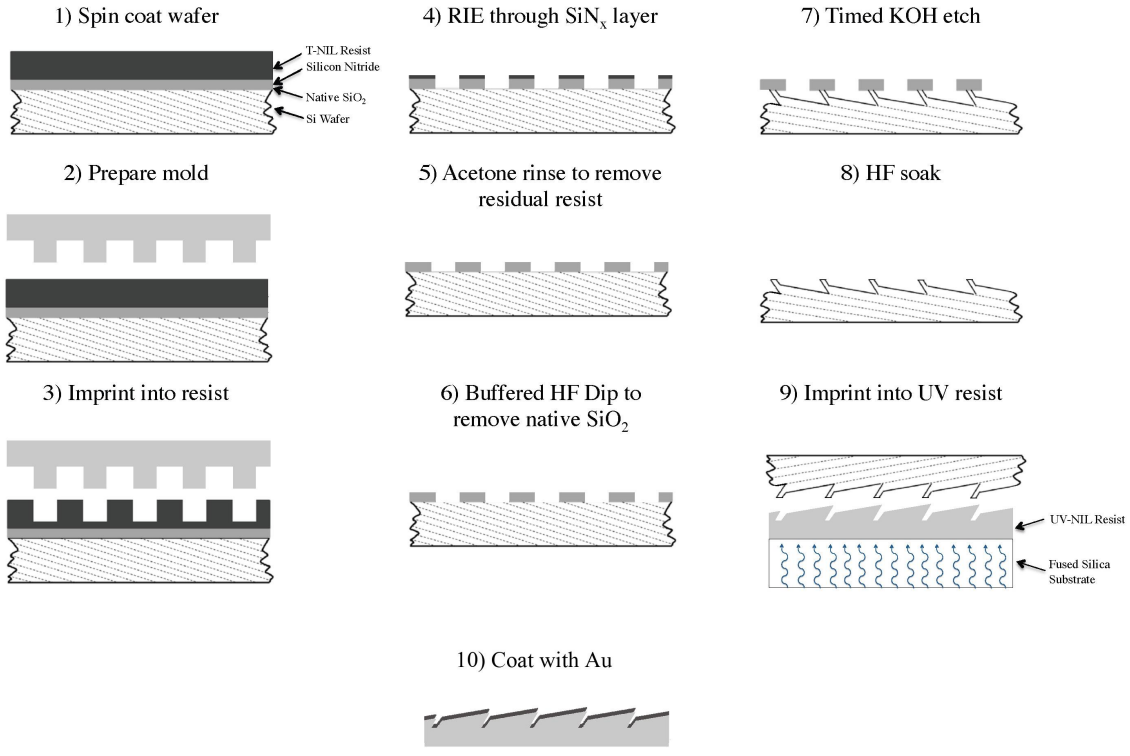

Figure 3.1. Procedure for fabricating off-plane gratings.[3]

4. DIFFRACTION TESTING

The process described in section 3 was used to fabricate a <100> grating with radial groves at an average density of 6033 grooves/mm and a facet angle of 54.7°. For preliminary qualification, this grating was tested in a vacuum chamber at the University of Iowa using a Manson Mg Kα X-ray source as shown in Figure 4.1. A series of slits along the beam-line is used to sculpt a 1 by 1 mm square X-ray beam. Using a linear stage, the grating is moved into the beam and a rotational stage allows the grating to be zeroed in rotation then set to a desired graze angle η. The grating reflects and diffracts light onto a CCD. The CCD is on a detector table that can translate along the direction of the incident beam to increase or decrease the throw, L, of the system. In addition, the CCD is equipped with two orthogonal linear stages (X and Y), allowing the full arc of diffraction to be mapped.

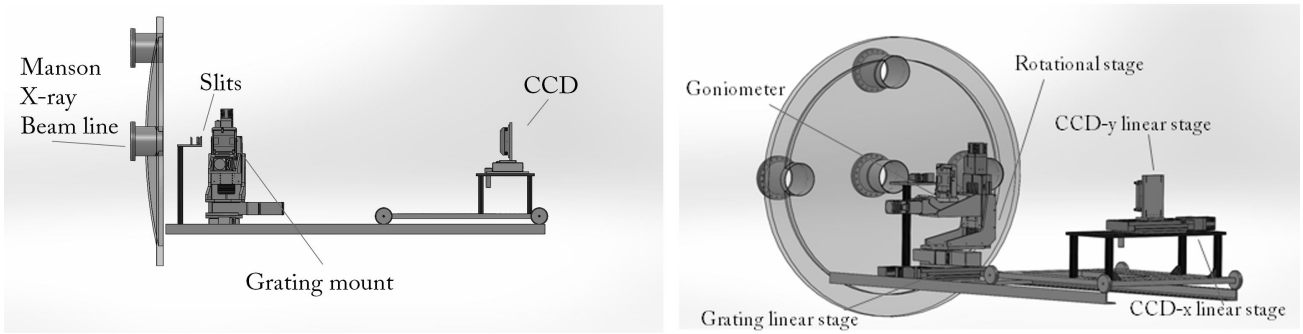

Figure 4.1. Chamber assembly for testing fabricated gratings.

The grating was mounted in the chamber with a graze angle of 0.83° and a throw of 1.1 m between the grating and the CCD. A series of CCD images were taken, creating a mosaic of the arc of diffraction shown in the left image of Figure 4.2. Knowing the throw, L, and groove density of the grating, D, the linear distance dispersed from zero order for different orders of diffracted light, n, can be calculated via Equation 1:

$$\frac{d\lambda}{d\mathrm{x}} = \frac{10^7}{nLD}\frac{\text{Å}}{\text{mm}}. \tag{1}$$

The dispersion for this chamber system is 1.51 Å/mm. Dividing the wavelength of Mg Kα line, 9.89 Å, by the dispersion of the system we find the physical separation of each order in the dispersion direction to be 6.55 mm. A series of 500 ten second exposures were taken at seven locations and combined to form the mosaic in the left of Figure 4.2. Using the central position of each order, the data were fit with a circle of radius 26.5 mm. From the fit equation of the circle and the position of zero order the angle α of the system is calculated to be 52.4° (See Figure 1.1). For perfect Littrow mounting, α would be identical to the facet angle (54.7 degrees). However, this mounting is close enough to the Littrow mount to exhibit a significant blaze effect. The right image of Figure 4.2 is a one-dimensional histogram of the left image binned along the CCD horizontal (cross-dispersion) direction. As the CCD horizontal direction is roughly aligned with the dispersion direction of the grating, the figure thus shows the intensity of the diffraction pattern as a function of the distance dispersed from zero order. The three peaks to the far left correspond to 7th order, 6th order and 5th order and represent an envelope of high efficiency caused by the grating being mounted near Littrow.

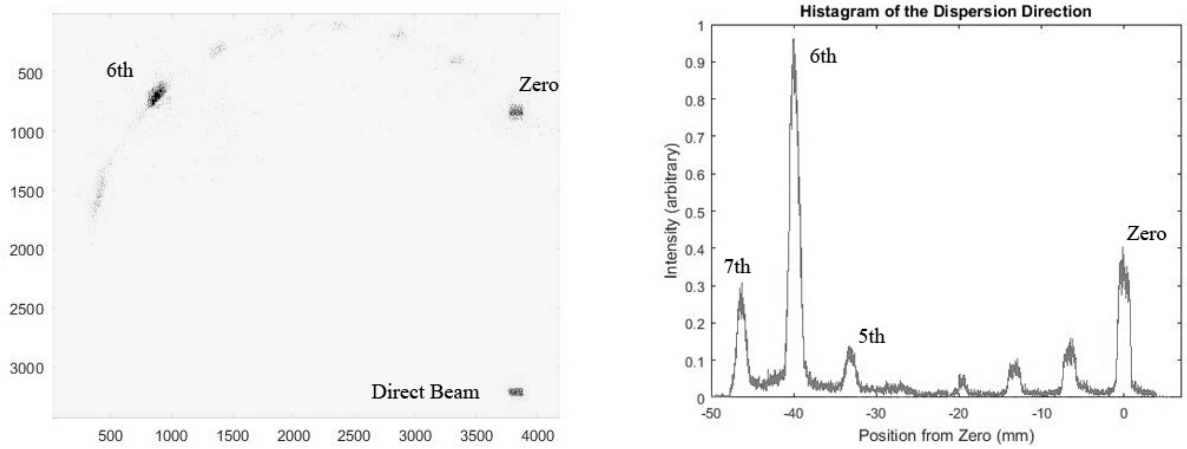

Figure 4.2. Left: A mosaic of seven CCD images showing the arc of diffraction of a <100> blazed grating with direct beam and zero order on the far right of the image. Right: A one dimensional compression of the left image along the dispersion direction with the direct beam removed. The data are scaled to an arbitrary intensity.

The intensity of each order in the histogram was fitted to a non-normalized Gaussian distribution using weights of $\sqrt{N}$, where N is the number of counts per bin. The resulting equations were integrated and divided by the total number of photons observed in all CCD exposures to give the relative efficiency of each order. The efficiencies are shown in Table 4.1. These results very closely match the theoretical curves predicted using PCGrate-SX v6.1 software. Figure 4.3 shows theoretical curves for a grating with identical facets and groove density as the fabricated grating and a surface roughness of 3 ± 1 nm. Plotted over the theoretical curves is the Mg Kα energy line. At this energy, 6th order is predicted to be the most efficient with other orders expected to be almost an order of magnitude less efficient. The collected data agree with the theoretical prediction in that significant signal is expected in 5th, 6th, and 7th orders, with the remaining orders being greatly suppressed. Unlike the PCGrate model, zero order shows high efficiency. This is believed to be caused by imprint fidelity issues due to particulate contamination during fabrication. The areas where the grating pattern was not properly transferred behave as a mirror, reflecting or scattering incident light rather than diffracting.

Table 4.1. The relative efficiency of each order calculated by the percentage of the intensity of diffracted light in each order vs. the total intensity of all diffracted light. These are crude efficiency measurements to test the blaze effect, dedicated efficiency measurements will be performed at a synchrotron facility.

Diffracted Order	**Relative Efficiency (%)**
0	~17%
1st	~6%
2nd	~4%
3rd	<1%
4th	<1%
5th	~5%
6th	~42%
7th	~10%

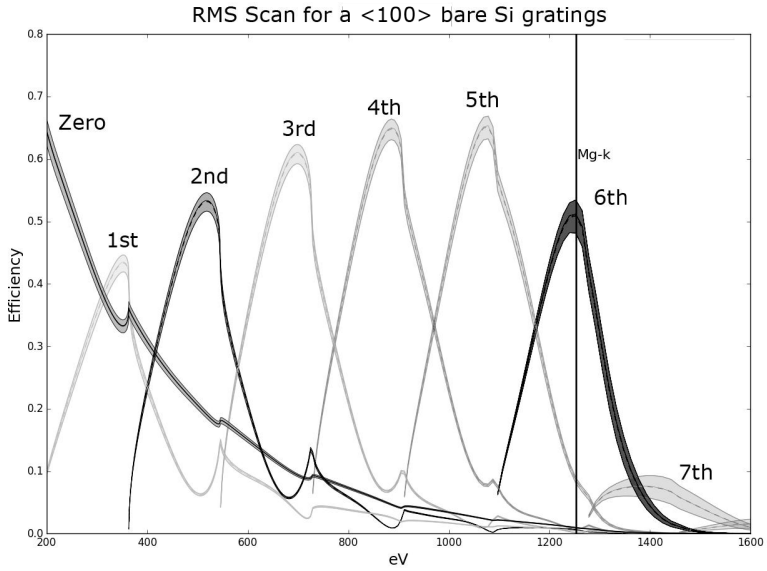

Figure 4.3. Theoretical curves of a <100> grating with a range of surface roughnesses tested in a mounting configuration identical to that of the X-ray qualification test. At Mg Kα line energies 6th order is predicted to have high efficiency with other orders greatly suppressed.

5. SUMMARY

In the context of future X-ray missions, X-ray grating spectrometers must be able to achieve high throughput and high spectral resolution. Our goal is to realize this performance by utilizing off-plane reflection gratings. We have produced a ten step grating fabrication technique that is capable of producing the radial, blazed, high density groove profile that is required to meet this goal. Using these techniques, a 54.7° blazed off plane grating with radial groves at an average density of 6033 grooves/mm has been produced. This grating was tested in an X-ray test chamber at the University of Iowa and has shown 42% relative efficiency in 6th order, which closely agrees with the theoretical predictions made using PCGrate-SX for such a grating aligned in the Littrow configuration. In the future, this grating will be sent to the BESSY II synchrotron facility for dedicated efficiency testing.

The next challenge will be to refine the fabrication process to eliminate imprint fidelity issues caused by particulate contamination. To do this, e-beam lithography will be used to write the laminar grating pattern into the resist layer. This will eliminate a majority of the imprint fidelity issues originating from particulates separating the mold from the substrate, as e-beam lithography does not rely on surface contact for pattern generation.

REFERENCES

[1] DeRoo, C., McEntaffer, R. L., Schultz, T., Zhang, W. W., Murray, N. J., O'Dell, S. L., and Cash, W., "Pushing the boundaries of x-ray grating spectroscopy in a suborbital rocket," in [*Society of Photo-Optical Instrumentation Engineers (SPIE) Conference Series*], *Society of Photo-Optical Instrumentation Engineers (SPIE) Conference Series* **8861**, 1 (Sept. 2013).

[2] DeRoo, C. T., "White paper: Primer: Off-plane diffraction grating theory," tech. rep., Department of Physics and Astronomy, University of Iowa.

[3] DeRoo, C. T., "White paper: Fabricating off-plane reflection gratings for use in a rocket-bourne x-ray spectrometer," tech. rep., Department of Physics and Astronomy, University of Iowa.

[4] Cash, Jr., W. C., "X-ray optics. II - A technique for high resolution spectroscopy," *Applied Optics* **30**, 1749–1759 (May 1991).

[5] DeRoo, C., McEntaffer, R., Miles, D., Peterson, T., Marlowe, H., Tutt, J., Donovan, B., Menz, B., Burwitz, V., Hartner, G., Allured, R., Smith, R., Gunther, R., Yanson, A., Vacanti, G., and Ackermanne, M., "Line Spread Functions of Blazed Off-Plane Gratings Operated in the Littrow Mounting," *Journal of Astronomical Telescopes, Instruments, and Systems* (Submitted 2015).

[6] McEntaffer, R., DeRoo, C., Schultz, T., Gantner, B., Tutt, J., Holland, A., O'Dell, S., Gaskin, J., Kolodziejczak, J., Zhang, W. W., Chan, K.-W., Biskach, M., McClelland, R., Iazikov, D., Wang, X., and Koecher, L., "First results from a next-generation off-plane X-ray diffraction grating," *Experimental Astronomy* **36**, 389–405 (Aug. 2013).

[7] Allured, R., Donovan, B. D., and McEntaffer, R., "Alignment tolerances for off-plane reflection grating spectroscopy: theoretical calculations and laboratory techniques," in [*Society of Photo-Optical Instrumentation Engineers (SPIE) Conference Series*], *Society of Photo-Optical Instrumentation Engineers (SPIE) Conference Series* **8861**, 1 (Sept. 2013).

[8] Allured, R. and McEntaffer, R. T., "Analytical alignment tolerances for off-plane reflection grating spectroscopy," *Experimental Astronomy* **36**, 661–677 (Dec. 2013).